Kinetics of electrochemical intercalation of lithium ion into $Li[Li_{0.2}Co_{0.3}Mn_{0.5}]O_2$ electrode from Li_2SO_4 solution

K.C. Mahesh[a*], G.S. Suresh[b]

a. Mount Carmel College, Autonomous, Vasanth Nagar, Bengaluru-560052, India.

b. Department of Chemistry and Research Centre, N.M.K.R.V. College for Women, Jayanagar, Bengaluru-560 011, India.

* Author for correspondence

Telephone: +91-80-22261759

Fax: +91-80-22286386

E-mail address: kcmahesh78@gmail.com (K.C. Mahesh)

Abstract

The kinetics of electrochemical lithium ion intercalation into $Li[Li_{0.2}Co_{0.3}Mn_{0.5}]O_2$ electrode in 2 M Li_2SO_4 aqueous electrolyte has been studied using two electroanalytical methods, namely, potentiostatic intermittent titration technique (PITT) and galvanostatic intermittent titration technique (GITT). The results are compared with those from nonaqueous electrolytes. Layered, lithium-rich $Li[Li_{0.2}Co_{0.3}Mn_{0.5}]O_2$ cathode material was synthesized by reactions under autogenic pressure at elevated temperature (RAPET) method. The effects of ohmic potential drop and charge-transfer resistance have been considered while predicting the current transients obtained with aqueous electrolyte. For PITT and GITT, we have defined their characteristic time-invariant functions, $It^{1/2}$ and $dE/dt^{1/2}$, respectively to present the diffusion time constant τ. Application of different theoretical diffusion models for treating the results obtained by the above-mentioned techniques allowed us to calculate the diffusion coefficient of lithium ions (D) at different potentials (E). The intercalation process is explained by considering the possible attractive interactions of the intercalated species in terms of Frumkin intercalation isotherm. We have observed a strict correspondence between the peaks of the intercalation capacitance and the minima in the corresponding log D vs. E curve.

Key words: Li-ion batteries, Lithium intercalation/de- intercalation reaction, PITT and GITT techniques, Chemical diffusion coefficient

Introduction

Rechargeable lithium-ion batteries are mainly used as the power source in modern portable electronic devices such as cellular phones, laptop computers etc., because of their high output voltage, high specific energy and long cycle life. Layered manganese-based oxide materials are of high fundamental and technological interest as cathode materials in lithium-ion batteries due to their high capacity, low cost, and less toxicity as compared to the commonly used $LiCoO_2$. Unfortunately, all pure or lightly doped layered forms of $LiMnO_2$ have been found to transform into defective spinel-related form on cycling with a significant change in voltage profile [1–3]. Further, $LiMnO_2$ is not thermodynamically stable at elevated temperature and cannot be synthesized by the same methods as used for other layered compounds. One of the methods to stabilize the layered structure of $LiMnO_2$ is to make the electronic properties of manganese to be more cobalt-like by substitution of manganese with more electron rich elements. Some research groups have attempted to stabilize manganese-based oxide solution between Li_2MnO_3 (or $Li[Li_{1/3}Mn_{2/3}]O_2$) and $LiMO_2$ (M = Ni, Co…) [4–6]. These lithium-rich compounds with layered structure show quite interesting electrochemical properties to the electrode material by improving structural stability by the formation of two component composite material. These oxides are derived from $Li[Li_{1/3}Mn_{2/3}]O_2$ by substitution of Li^+ and Mn^{4+} by Ni^{2+} or Co^{3+}, respectively, while maintaining the remaining Mn atoms in the 4+ oxidation state. $Li[Li_{1/3}Mn_{2/3}]O_2$ was considered electrochemically inactive because Mn^{4+} in $Li[Li_{1/3}Mn_{2/3}]O_2$ normally could not be oxidized beyond 4+ oxidation state in order to extract lithium from its lattice. The promising lithium-rich compounds have received particular attention in recent years because of their high capacity of ~300 mA h g^{-1}, nearly twice higher than the presently commercialized $LiCoO_2$ and $LiFePO_4$ cathodes [7–10].

$Li[Li_{0.2}Co_{0.3}Mn_{0.5}]O_2$ compound has a layered oxide lattice based on a hexagonal α-$NaFeO_2$ structure belonging to *R3m* space group. The stoichiometry of $Li[Li_{0.2}Co_{0.3}Mn_{0.5}]O_2$ can be determined from the assumption that transition metals Co and Mn are in the oxidation states of 3+ and 4+, respectively. These compounds are regarded as a solid-solution series between $LiCoO_2$ and $Li[Li_{1/3}Mn_{2/3}]O_2$. The weak peaks between 20° and 25° in the XRD pattern of this compound are reflected by a monoclinic unit cell with a *C2/m* symmetry rather than a *R3m* lattice, due to a $LiMn_6$ cation arrangement that occurs in the transition metal layers of Li_2MnO_3 regions. Therefore, the layered $Li_{1+x}MO_2$ materials can be alternatively represented in a two component "composite" notation as $xLi_2MnO_3(1-x)LiMO_2$. The appearance of small peaks is also attributed to the super lattice ordering of Li and Mn in the transition-metal layers. These super lattice peaks have been observed in the XRD patterns of Li_2MnO_3-based oxides. When the Co content of compound increases, these peaks become broad or disappear because the 1:2 ordering of Li and Mn is destroyed by Co substitution. We can assume that Li is in the 3*a* sites, Co^{3+}, Mn^{4+} and Li^+ are in the 3*b* sites, and oxygen is in the 6*c* sites. Since, the radii of Co^{3+} (0.54 Å) and Mn^{4+} (0.53 Å) are much smaller than that of Li^+ (0.76 Å), no Co^{3+}, Mn^{4+} are expected to be in the 3*a* sites of Li [11].

The most interesting feature of the solid solution series between $Li[Li_{1/3}Mn_{2/3}]O_2$ and $LiMO_2$ is their discharge capacity, which is higher than the theoretical value. For example, according to Lu et al., $Li[Li_{0.113}Ni_{0.33}Mn_{0.556}]O_2$ exhibited an initial charge capacity of ~280 mA h g^{-1} between 2.0 and 4.8 V [12]. However, the theoretical capacity of the material for the Ni^{2+}/Ni^{4+} redox couple is only 200 mA h g^{-1}. It is curious to know that where the extra capacity originates. It was explained that during the first charge the material first reach the theoretical capacity of 200 mA h g^{-1}, at 4.45 V and then further Li extraction from the Li layer was compensated by oxygen loss so that the final composition was reached at 4.8 V [5]. Another possible explanation for the extra capacity is participation of oxygen ions in the

redox reactions. Oxygen ions also contribute to the charge compensation during deintercalation of lithium ions [13].

In spite of their exceptional high capacity and low cost, the $x\mathrm{Li}[\mathrm{Li}_{1/3}\mathrm{Mn}_{2/3}]\mathrm{O}_2(1-x)\mathrm{LiMO}_2$ solid mixtures suffer from two major disadvantages of low initial coulombic efficiency and poor rate capability, which bring about great difficulties for practical applications [14]. Although there has been no definite evidence presented so far, the large initial irreversible capacity loss is usually attributed to an irreversible removal of partial lithium as $\mathrm{Li}_2\mathrm{O}$ from the crystal lattice along with an elimination of the oxygen vacancies produced during first charge. This lead to a reduction of the effective sites for accommodating the lithium ions in subsequent cycles [15]. Similarly, several mechanisms, such as the formation of a thick solid-electrolyte interface (SEI) on the cathode surface and the frustrated diffusion of lithium ions in the rearranged lattice formed during the first charge, have been proposed to account for the low-rate capability of the $\mathrm{Li}_2\mathrm{MnO}_3\cdot\mathrm{LiMO}_2$ materials, but the rapid capacity fading of the materials with increased charge and discharge rate is not fully understood [16–19].

The charging and discharging of rechargeable lithium-ion batteries involves lithium ion transfer from one ion insertion electrode to another one. This transfer can be considered as a topotactic intercalation reaction, meaning that the guest ions occupy the interstitial sites of both crystalline host matrices and that their charging and discharging result in a non-uniform concentration profile in the electrode bulk [20]. The process of ion insertion into host electrodes that have been polarized in solutions can be regarded as first order phase transition. The thermodynamic driving force for the phase transition during ion intercalation has been discussed by McKinnon and Haering within the framework of lattice gas models [21]. It was demonstrated that highly attractive short-range interactions between the intercalation sites results in the appearance of a high maximum on the non equilibrium electrochemical free energy curve as a function of the intercalation level. However, as

thermodynamic analysis does not provide an answer to the question of what kind of relaxation processes determine the rate of phase transition; kinetic analysis is required [22]. McKinnon and Haering have suggested that slow solid-state diffusion is, presumably, the rate-determining step for phase transition. Using a phase -field model, Han et al. [20] have presented a comprehensive view of how the existence of the spinodal domain (describing the transformation of a system of two or more components in a metastable phase into two stable phases) in the free energy curve affects the applicability of classical electroanalytical techniques for the determination of the chemical diffusion coefficient, *D*. Numerical calculations of the dependence of *D* on the intercalation level, using the energy gradient coefficient values, have confirmed that the incremental titration techniques such as PITT and GITT are valid for the metastable domain, in close proximity to the spinodal domain itself. In this regard, we have investigated the kinetics of electrochemical intercalation of lithium ion into $Li[Li_{0.2}Co_{0.3}Mn_{0.5}]O_2$ electrode from an aqueous 2 M Li_2SO_4 electrolyte with the help of PITT and GITT. PITT and GITT, with small potential and current steps, respectively, are the most appropriate tools for measuring the entire sequence of rate-determining steps of phase transitions as a function of time. Further, from the electrochemical point of view, the cathodes for lithium-ion batteries are not well defined systems. They are usually composite electrodes containing the active material, a polymeric binder such as PVDF, PTFE etc. and an electrically conductive additive like carbon black, graphite etc., whereas most of the theoretical approaches are applicable to strictly homogeneous thin film electrodes. Application of different techniques like PITT and GITT with overlapping characteristic time windows increases the reliability of the various calculated parameters related to lithium-ion intercalation, such as diffusion coefficient and intercalation capacitance. The goal of this paper is to investigate the kinetics of the solid-state diffusion of lithium ions in

$Li[Li_{0.2}Co_{0.3}Mn_{0.5}]O_2$ electrode, in addition to their equilibrium and quasi-equilibrium characterization from an aqueous electrolyte.

Theory

Potentiostatic intermittent titration technique

PITT, an extension of potential-step chronoamperometry, was first introduced by Wen et al. [23] for characterization of intercalation electrodes by the chemical diffusion coefficients of intercalate species. Here we discuss only the relevant part of the technique used in the analysis of the kinetic data of lithium ion in lithium intercalation electrodes. In chronoamperometry, a constant potential is applied, and the resulting current response is measured as a function of time. As mass transport under these conditions is solely controlled by diffusion, the current-time curve reflects the change in the concentration gradient in the vicinity of the surface. This involves a gradual expansion of the diffusion layer associated with the depletion of the reactant, and hence decreased slope of the concentration profile as time progresses. Accordingly, the current decays with time as given by the Cottrell equation:

$$I = nFA\Delta CD^{1/2}/\pi^{1/2}t^{1/2} = kt^{-1/2} \quad (1)$$

where, n is the number of electrons per reaction, F is Faraday constant, A is the surface area of the electrode, D is the diffusion coefficient of lithium ion in the solid state and ΔC is the difference between the equilibrium concentrations at the values of potential after and before the potential step. It follows from the above equation that, under infinitely fast kinetics and linear diffusion in semi-infinite systems, the current response to a potential step plotted as I vs. $t^{-1/2}$ yields a straight line. Such an $It^{1/2}$ constancy is often termed "Cottrell behavior". Rearranging Eq. 1 yields:

$$D^{1/2} = It^{1/2}\pi^{1/2}/nFA\Delta C \quad (2)$$

In a linear system the charge ΔQ transferred into the electrode during the potential step is given by [24]

$$\Delta Q = nFA\Delta Cl, \quad (3)$$

where l is the intercalation length. It follows from Eqs. 2 and 3 that:

$$D^{1/2} = It^{1/2}\pi^{1/2}l/\Delta Q \quad (4)$$

This expression can be used to evaluate the diffusion coefficient from a potential-step current response in a linear system. A parameter often used in this context is the diffusion time constant $\tau = l^2/D$, where intercalation length l is set equal to the radius of the active particles. The cross-sectional area for lithium diffusion is the envelop of facets perpendicular to the basal planes of the particles, and the insertion of lithium takes place independently, in parallel with the particle. Thereby, the average intercalation length for each electrode should be taken as half of the particles' average size (assuming that solid-state diffusion takes place in each particle from its facets to the centre). The constant value of $It^{1/2}$ in Eq. 1 is equal to the slope of the tangent to the I vs. $t^{-1/2}$ curve going through the coordinate origin [24]. This can be understood by considering that the slopes of straight lines going through the origin and different points of the I vs. $t^{-1/2}$ curve are given by $I/t^{-1/2} = It^{1/2}$. Among these straight lines, the one acting as an upper tangent to the I vs. $t^{-1/2}$ curve exhibits the largest slope and hence the largest value of $It^{1/2}$. This region is often referred as Cottrell region. Analytical applications of chronoamperometry rely on pulsing of the potential of the working electrode repetitively at fixed time intervals. The analysis of the current-time curves can be carried out by plotting $It^{1/2}$ vs. log t. Therefore, the Cottrell behavior, in $It^{1/2}$ vs. log t plot, would correspond to a plateau. The shape of the curves reflects the succession of several phenomena, separated according to their time domains. A detailed explanation of the occurrence of different regions in the $It^{1/2}$ vs. log t plot during a small potential step is described in the discussion part of this paper. $It^{1/2}$ vs. log t representation is a convenient way to plot the chronoamperometric response mainly because the different time domains are well evidenced in these plots while in the I vs. t plot they appear overlapped [25]. In particular, the

physical phenomena of ion diffusion and accumulation into the electrode are easily evidenced. The plateau describes the semi-infinite planar diffusion ($t << \tau$, $\tau = l^2/D$, where t is the time elapsed from the beginning of the potential step) and represents the Cottrell behavior. The following region, when the absolute value of $It^{1/2}$ decreases, represents the finite-space diffusion ($t >> \tau$), i.e., ions accumulation into the composite electrode. The two regions are separated by the characteristic diffusion time τ, which can be approximated by the middle time point. It is possible to calculate D from the estimated values of τ.

Galvanostatic intermittent titration technique

Weppner and Huggins [26] first introduced GITT to investigate the thermodynamic and kinetic properties of solid mixed-conducting materials. In a galvanostatic mode, a constant current (I) is applied to the test cell for some time interval (τ), which causes a time-dependent concentration gradient of the active species in the electrodes just inside the interface with the electrolyte. The change in the cell voltage (E) is measured as a function of time (t). To calculate the surface concentration (and hence the potential) as a function of time, under the applied current, assuming constant diffusivity of the diffusing species and semi-infinite solid, the time dependence of the concentration C at the interface x has to be determined by solving Fick's second law with appropriate boundary conditions:

$$\partial C(x,t)/\partial t = D\partial^2 C(x,t)/\partial x^2 \quad (5)$$

By measuring the electrode potential versus a reference electrode after the imposition of a small galvanostatic pulse, we can determine the potential change with time. The slope of the potential versus square root of time curve will be used to determine the diffusion coefficient of the lithium ion in the electrode. The chemical diffusion coefficient D can be calculated using the fundamental equation [20]:

$$D = 4/\pi(1/nFA)^2[I(\mathrm{d}E/\mathrm{d}c)/(\mathrm{d}E/\mathrm{d}t^{1/2})]^2 , \quad t << \tau \quad (6)$$

where, all the parameters have their usual meaning. For small currents and short time steps t', $dE/dc \approx \Delta E_s/\Delta c$ and $dE/dt^{1/2} \approx \Delta E_t/t'^{1/2}$, where ΔE_s is the difference in open circuit voltage measured at the end of two sequential open-circuit relaxation steps and ΔE_t stands for the total transient potential change after time t'. With these relations and by relations between the quantities of n, F, A and I, Eq. 6 is transformed into a simpler form [20]

$$D = (4l^2/\pi t')(\Delta E_s/\Delta E_t)^2, \quad t << \tau \tag{7}$$

where, ΔE_t is the total transient voltage change of the cell for applied current for time t' and ΔE_s is the change of the steady-state voltage of cell for this step. However, the diffusion coefficient values calculated using the above equation from GITT data are not error free. These deviations come from several assumptions used to derive a tractable expression for experimental analysis [20]. Some of the approximations that are responsible for the intrinsic errors to the GITT method are:

1. *One-dimensional semi-infinite particles*: GITT assumes particles with simple geometries (i.e. one dimensional, cylindrical, or spherical geometries) that are large enough such that finite size effects can be neglected.

2. *Fickian dynamics*: GITT assumes that the transport is described by Fick's equation, with no gradient energy term.

3. *Constant D during perturbation*: GITT assumes that during the current pulse the diffusion coefficient does not change as the concentration changes.

4. *Constant* dE/dc and $dE/dt^{1/2}$: GITT assumes these deviations are constant to make it possible to write the diffusion coefficient in terms of experimentally accessible quantities.

In the potentiostatic current transient measurements like PITT, the initial and boundary conditions ($t = 0$ and $t = t$) usually satisfying Fick's second law are not exactly fulfilled. The applied potential step during the current transient $t = t$ oscillates severely around the steady-state, thus creating a large transient polarization effect. This fall short leads to a deviation

from the linear relationship in the I vs. $t^{-1/2}$ curve, in the short time range, represented by the steady-state condition theoretically expected. This makes the potentiostatic current transient technique inaccessible to the accurate determination of the kinetic data such as diffusion coefficient [27]. In contrast, GITT places no oscillations on the initial and boundary conditions for Fick's law and hence give a linear relationship between potential and square root of time in the short time range of the galvanostatic potential transient. In brief, careful study of potential-time dependencies of lithium intercalation processes during small current pulses which changes the potential in small increments may provide a clue for understanding the mechanisms of intercalation process in which phase transitions are involved.

Experimental

Stoichiometric amounts of LiOH, Co_3O_4 and MnO_2 were weighed, mixed and ground well. The resulting powder was introduced into a 5 mL Swagelok cell. The Swagelok cell parts consist of a small threaded stainless-steel tube closed by two caps from both sides. The filled Swagelok cell was closed tightly and then placed inside an alumina pipe in the middle of the furnace. The temperature was raised to 600 °C at a rate of 10 °C/minute and held at this temperature for 14 hours. The chemical dissociation and transformation reaction takes place under the autogenic pressure of the precursor at the fixed temperature. The Swagelok cell is allowed to cool gradually to room temperature, opened and the obtained product was used after grinding.

Electrodes were prepared by using stainless steel mesh as a current collector. The mesh was cut into circular shape of about 1 cm^2 area and welded with stainless steel wire for electrical contact. The mesh was sandblasted to remove the oxide layer, washed with water, rinsed with acetone, dried, and weighed. Cathode and anode materials were prepared in the same way. Powder mixture of the sample, carbon black and polyvinylidene fluoride in the weight ratio 75:20:5 was ground in a mortar; a few drops of *N*-methyl-2-pyrrolidone (NMP) were added to

get slurry. The slurry was coated onto the pretreated mesh and dried in a vacuum oven at 110 °C overnight.

A three-electrode electrochemical cell was employed for cyclic voltammetry (CV) in aqueous 2 M Li_2SO_4 solution. A saturated calomel electrode and Pt foil were used as reference and counter electrodes respectively. The three-electrode electrochemical cell for the PITT and GITT measurements was similar to that used for the CV studies. For potentiostatic titration of the electrode, potential steps of variable amplitude were used. Near incremental capacity peaks, the incremental potential step was as small as 10 mV. The duration of each potential step (typically 3600 s) was long enough to enable the reaching of full equilibration of the electrodes. Each subsequent potential step was applied after complete equilibration during the preceding step. Up to 30 titrations covering the whole range of intercalation potentials of $Li[Li_{0.2}Co_{0.3}Mn_{0.5}]O_2$ electrode were performed. To obtain equal potential increments during both PITT and GITT, we used 0.1 mA amplitude GITT for 600 s followed by a relaxation time of 3600 s. This time was sufficient to allow for a flat concentration profile of all the species all over the entire sample thickness. Current pulses were applied from initial equilibrium potentials until the predetermined new potential values were reached, which differed from the initial ones by the same increments relevant to the set of PITT measurements with the same electrode. As the target potentials were reached, the electrode was further polarized at these potentials until the current was dropped close to zero. All the experiments of $Li[Li_{0.2}Co_{0.3}Mn_{0.5}]O_2$ in nonaqueous electrolyte were carried out in the same way. The test cell was prepared with Li metal foil as reference and counter electrodes, and a 1 M $LiAsF_6$ dissolved in EC+DMC (1:1 v/v) as the electrolyte solution. Celgard 2340 was used as the separator. Assembling of the cell was carried out in a glove box filled with argon gas. All the electrochemical measurements were made using a Biologic potentiostat-galvanostat instrument.

Results and discussion

CV studies

Figure 1a shows the cyclic voltammogram of $Li[Li_{0.2}Co_{0.3}Mn_{0.5}]O_2$ prepared by reactions under autogenic pressure at elevated temperature method in 2 M Li_2SO_4 aqueous solution at a scan rate of 0.1 mV s^{-1} between 0.0 and 1.2 V. There is a pair of sharp anodic and cathodic peaks located at 0.66/0.63 V corresponding to lithium intercalation and deintercalation of $Li[Li_{0.2}Co_{0.3}Mn_{0.5}]O_2$ electrode. The anodic peak appears due to the oxidation of cobalt ions from Co^{3+} to Co^{4+} accompanied by the deintercalation of equal number of lithium ions. The cathodic peak is due to the reduction of cobalt ions accompanied by the intercalation of lithium ions. The redox couple at 0.66/0.63 is related to the existence of a two-phase domain of $Li[Li_{0.2}Co_{0.3}Mn_{0.5}]O_2$. These measurements indicate a distinct phase change occurring as the amount of lithium is electrochemically varied between 1 and 0.6 $\{Li[Li^{+}_{0.2}Co^{3+}_{0.3}Mn^{4+}_{0.5}]O_2 \rightarrow Li_{0.6}[Li^{+}_{0.2}Co^{4+}_{0.3}Mn^{4+}_{0.5}]O_2 + 0.4Li\}$. Figure 1b shows the CV profile of $Li[Li_{0.2}Co_{0.3}Mn_{0.5}]O_2$ obtained in the nonaqueous electrolyte at a scan rate of 0.1 mV s^{-1} using lithium foil as counter and reference electrodes. The cell was cycled in the range from 3.0 to 4.2 V (vs. Li / Li^{+}). A pair of redox peaks at 3.85 and 3.55 V which correspond to the lithium ion deintercalation-intercalation are observed. It can be seen clearly that in the non-aqueous solution the current response of the redox reaction is much lower than that in the aqueous electrolyte solution due to the low ionic conductivity of organic-based solutions. The solvation of lithium ions in the organic solvent with high dipole moment and the resistance offered by the surface layer for lithium ion migration will have a retardation effect on the kinetics of lithium ion insertion from the nonaqueous electrolyte.

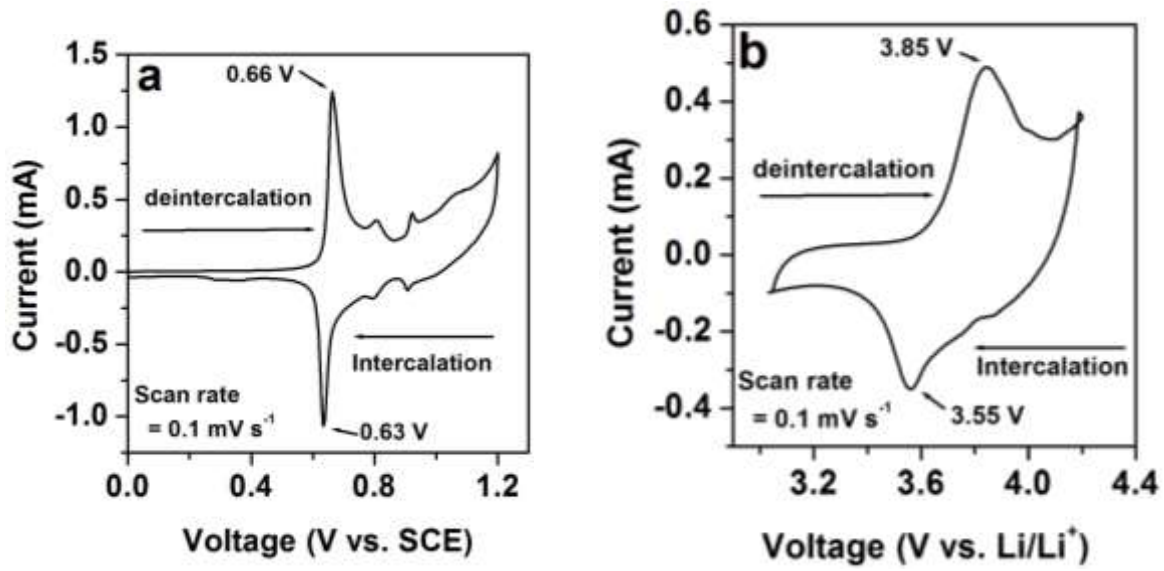

Figure 1. CV of $Li[Li_{0.2}Co_{0.3}Mn_{0.5}]O_2$ in (a) 2 M Li_2SO_4 aqueous electrolyte (b) 1 M $LiAsF_6$ / EC+DMC nonaqueous electrolyte at a scan rate of 0.1 mV s^{-1}.

PITT studies

Figure 2a shows the typical chronoamperometric response of a potential step from 0.63 to 0.61 V applied to $Li[Li_{0.2}Co_{0.3}Mn_{0.5}]O_2$ electrode in 2 M Li_2SO_4 aqueous electrolyte. The corresponding $It^{1/2}$ versus log t plot is shown in Figure 2b. The shape of this curve reflects the succession of several phenomena, separated according to their time domains. A detailed explanation of the occurrence of different regions in the chronoamperometric response during a small potential step was reported by Aurbach et al. [28]. These authors have well underlined how $It^{1/2}$ vs. log t representation is a convenient way to plot the data mainly because the different time domains are well evidenced in this plot while they appear overlapped in I vs. t plot. The lithium intercalation with the functional dependence of $It^{1/2}$ on log t reflects different kinetic regions of the entire intercalation process. Hence, using the time dependence of the product $It^{1/2}$, one can easily distinguish the regions in which the current decrease is linked to the corresponding increase of the diffusion layer thickness. We can expect the appearance of different time domains corresponding to the separate steps of the entire intercalation process, from the general features of the electrochemical intercalation

process. In fact, six different kinetic regions may be recognized as shown in Figure 2b. Region A corresponds to the interfacial charging of both current collector–electrode material and electrode material–solution interfaces. However, chronoamperometry can hardly provide enough time resolution to separate the corresponding time constants of these charging processes. Region B is characterized by a minimum with constant values of $It^{1/2}$, and hence this region reflects the Cottrell behavior, i.e., the short-time semi-infinite planar diffusion ($t << \tau$). However, the related Cottrell relationship is expressed by a shallow peak rather than a horizontal straight line. In this region, the time domain in which $It^{1/2}$ is approximately independent of log t (the Cottrell region) extents from 3 to 6 s, as shown in Figure 2b. Eq. 4 shows that D can be calculated either from the plateau of $It^{1/2}$ vs. log t plot {Figure 2b, region B} or, evidently, from the slope of the linear plot I versus $t^{-1/2}$ shown in Figure 2c. Calculation of D using Eq. 4 yields $D = 2.495 \times 10^{-10}$ cm^2 s^{-1} and $\tau = 40.08$ s. The characteristic diffusion length l is approximated here as half of the average particle size ($l = 1$ μm). Region D represents the long-term behavior of the chronoamperometric response corresponding to the finite space-diffusion ($t >> \tau$), i.e., ions accumulation into the composite electrode. For the time domain of $t >> \tau$, the current is dependent on the time according to the following equation [29]:

$$\log I = \log (2\Delta QD/l^2) - (\pi^2 Dt/4l^2) \quad (8)$$

According to Eq. 8, there are two ways to calculate the diffusion coefficient: (i) from the intercept of the log I vs. t curve, considering the amount of injected charge ΔQ, using the first part of the equation, or (ii) from the linear slope of the log I vs. t curve using the last part of the equation, without knowing ΔQ. As the precise measurement of ΔQ is difficult, the latter approach is more suitable for this purpose. Figure 2d shows the corresponding log I vs. t curve. The D value calculated from the linear slope of log I vs. t curve was found to be 2.20 ×

10^{-10} cm^2 s^{-1} and demonstrate a quite reasonable match between the values calculated from both the short and long-time domains (regions B and D). Region C is an intermediate (boundary) region between the short and long-time diffusion regions B and D. Region E also characterizes an intermediate stage which precedes the establishment of the new equilibrium state corresponding to the potential applied. Region F indicates the completion of the intercalation process, i.e., establishment of equilibrium state throughout the bulk of $Li[Li_{0.2}Co_{0.3}Mn_{0.5}]O_2$ layered structure. At equilibrium, we would expect the value of $It^{1/2}$ to drop to zero, since the net passing current approaches zero. However, Figure 2b shows that this is not true. This may be due to a small and constant background current which is due to some continuous reduction of solution species. When this reduction reaches a steady state, $It^{1/2}$ decreases with log t. Further, one can observe that a major part of region F looks like a Cottrell region (constant $It^{1/2}$ vs. log t), although it is not. This pseudo-Cottrell behavior results from the compensation of the decrease in current by the corresponding increase in the magnitude of $t^{1/2}$ value.

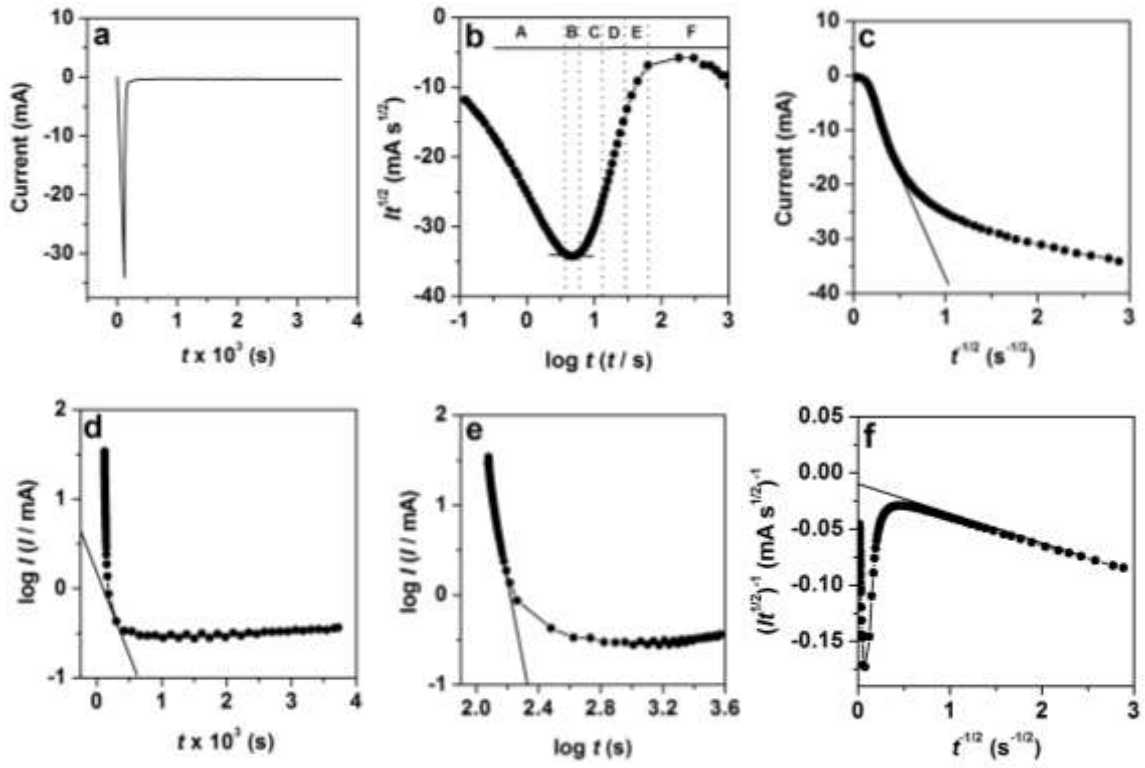

Figure 2. (a) Typical chronoamperometric curve of $Li[Li_{0.2}Co_{0.3}Mn_{0.5}]O_2$ electrode in 2 M Li_2SO_4 aqueous electrolyte. The potential step used was 0.63 to 0.61 V. (b) $It^{1/2}$ vs. log t plot calculated from the data of Figure 2a. Separate kinetic regions are marked by letters A to B. (c) I vs. $t^{-1/2}$ (d) log I vs. t (e) log I vs. log t and (f) $(It^{1/2})^{-1}$ vs. $t^{-1/2}$ plots calculated from the data of Figure 2a.

Figure 2e shows log I vs. log t plot of the same chronoamperometric response. The plot exhibits a first order exponential decay with almost zero slopes in the long-time domain. The decrease in the absolute value of log I with time is due to the slow interfacial charge-transfer kinetic control. Usually, I vs. t curves in logarithmic plots are Z-shaped [30]. It is caused by the time difference between the inhibiting components. The upper horizontal fragment illustrates the limitation of current by solid electrolyte interface resistance. The presence of this passive surface layer is the most important factor governing the electroanalytical performance of lithium insertion electrodes. The electrochemical intercalation from solution into the electrode is accompanied by the surface formation of this ion-conducting passive layer, with a high electric resistance. The sloping fragment represents the diffusion control.

The lower horizontal part of the curve depicts the constant phase transition rate on the internal boundary. The current vanishes once this phase transition is over. In our work, as seen in Figure 2e, the upper horizontal part which describes the kinetic limitation of current by SEI resistance is absent indicating SEI is not formed on $Li[Li_{0.2}Co_{0.3}Mn_{0.5}]O_2$ in presence of aqueous Li_2SO_4 electrolyte. We observed a sloping fragment describing the diffusion process. However, the lower horizontal part does exist indicating a constant phase transition rate at the internal boundary.

When diffusion is the only rate determining step of the overall lithium insertion process, then according to Eq. 1, $It^{1/2}$ vs. log t presents a characteristic time-invariant but potential dependent constant i.e., a plateau representing Cottrell behavior. However, from Figure 2b it is clearly seen that a sharp minimum rather than a horizontal time-dependent plateau is observed (region B). This can be attributed to the fact that diffusion is not the only single step controlling the rate, which in turn indicates the involvement of ohmic resistances, kinetic limitations, and slow finite-space diffusion in the lithium insertion process. Further evidence for the involvement of ohmic resistances and kinetic limitations in the insertion reaction can be ascertained from I vs. $t^{-1/2}$ plot shown in Figure 2c. The tangent line passing through the origin represents pure diffusion-controlled process calculated from Eq. 1. The deviation of experimental points from the tangent line which describes pure diffusion-controlled process also provides another evidence for considering the involvement of ohmic resistances and kinetic limitations. Thus, treating the experimental data with the classical equation implies that the response of the insertion electrode cannot be simply assigned to the diffusion control. At very short-times, other limitations like ohmic drops in the solution and in the bulk of the electrode material or slow interfacial charge transfer kinetics may control the rate of the reaction.

Considering the advantages and disadvantages of all known models, Montella [31] carefully analyzed how the above limitations influence both short-time and finite-space domains of diffusion, proposing several useful graphical modes for the calculation of the deviation of the measured chronoamperometric responses from a classical finite space diffusion behavior. However, quantitative estimations of these effects require a relatively complicated fitting procedure for experimental chronoamperomeric curves in both short-and long-time domains. To account for the above effects, Vorotyntsev et al. [32] later proposed a very simple approach for the correction of chronoamperometric data, measured from ion insertion electrodes, in which the solid-state diffusion process is complicated by slow interfacial kinetics and derived the following equation for short time interval ($t << \tau$) for processing the experimental PITT data.

$$I = \Delta Q[\Lambda^{-1}\tau + (\pi t\tau)^{1/2}]^{-1} \quad (9)$$

where, Λ is a dimensionless parameter; the ratio of the diffusion resistance to the total external resistance ($\Lambda = R_d/R_{ext}$, R_{ext} is generally composed of ohmic resistance, R_Ω and the interfacial exchange resistance, R_{ct}). The parameter Λ, quantitatively describes the effects of ohmic potential drops and slow charge-transfer kinetics on the diffusion process. Eq. 9 implies the use of a different coordinate system, $It^{-1/2}$ versus $t^{-1/2}$ for the treatment of experimental data, in which the slope of the curve gives $\tau/\Lambda\Delta Q$ while the intercept is equal to $(\pi\tau)^{1/2}/\Delta Q$. Figure 2f shows experimental plot of $It^{-1/2}$ versus $t^{-1/2}$ obtained from $Li[Li_{0.2}Co_{0.3}Mn_{0.5}]O_2$ electrode in 2 M Li_2SO_4 for a potential step from 0.63 to 0.61 V. From the slope and intercept of this graph in inverse coordinates, we have calculated the characteristic diffusion time constant, τ and the dimensionless kinetic parameter, Λ. From the intercept of the straight line on the ordinate axis in Figure 2f, the calculated τ is found to be 40.46 s which is close to the τ value (40.08 s) determined from the $It^{1/2}$ vs. log t curve in

Figure 2b. The related chemical diffusion coefficient calculated from Eq. 9 was 2.671×10^{-10} cm^2 s^{-1}. The dimensionless kinetic parameter Λ, was determined from the slope of the straight line and it was found to be 0.826. These results show that the above additional effects (ohmic potential drops and slow charge-transfer kinetics) are not markedly modifying the found values of D based on the pure diffusion model. Further investigations involving the primitive and advanced PITT data treatments are needed to elucidate the details.

To study the dependence of the chemical diffusion coefficient on the intercalation level, small potential steps were applied to $Li[Li_{0.2}Co_{0.3}Mn_{0.5}]O_2$ electrode during the course of lithium intercalation. The $It^{1/2}$ vs. log t curves of the corresponding chronoamperometric responses are shown in Figure 3. The shapes of all the $It^{1/2}$ vs. log t curves shown in Figure 3 are qualitatively similar to each other, regardless of the potential applied. However, $It^{1/2}$ shows a marked dependence on the electrode potential. The $|It^{1/2}|$ shows a maximum at 0.63 V which correspond to the CV peak potential, whereas on the tail ends of the peak $It^{1/2}$ tends to decrease. This trend can be explained based on Eq. 4 and Figure 1a. The voltammetric peaks shown in this figure are very narrow, and hence ΔQ increases drastically and then decreases when moving from right to left. As the potential dependence of $D^{1/2}$ is not as steep as that of ΔQ, the potential dependence of $It^{1/2}$ and ΔQ also should be essentially the same. In addition, the duration of the Cottrell region is also not constant. Going from the foot of the peak towards its maximum the Cottrell region shrinks suggesting that for potentials where the current flow reaches its maximum value, the lithium diffusion tends to reach a space-limited diffusion regime.

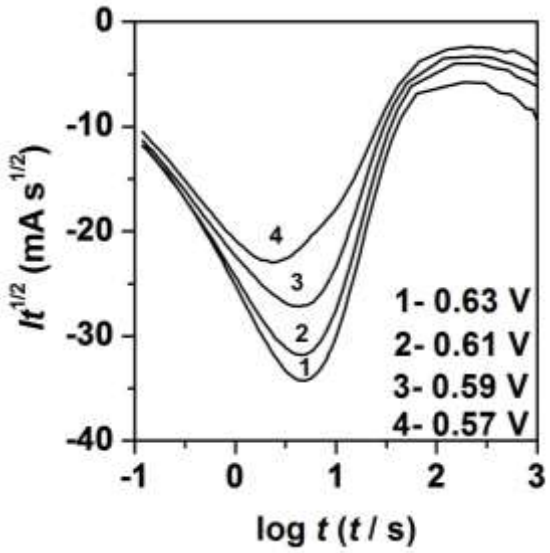

Figure 3. $It^{1/2}$ vs. log t plots for $Li[Li_{0.2}Co_{0.3}Mn_{0.5}]O_2$ electrode measured in 2 M Li_2SO_4 for small potential steps applied around voltammetric peak potentials.

For comparison, we have also carried out the same experiments for lithium ion intercalation into $Li[Li_{0.2}Co_{0.3}Mn_{0.5}]O_2$ electrode in presence of nonaqueous electrolyte, $LiAsF_6$/EC+DMC. Figure 4 shows the current-time responses obtained from the $Li[Li_{0.2}Co_{0.3}Mn_{0.5}]O_2$ electrode in the organic electrolyte. Qualitatively, the chronoamperometric responses measured with the organic electrolyte are similar to that described with aqueous electrolyte. However, the current response obtained, and the corresponding kinetic parameters evaluated with nonaqueous electrolyte are quantitatively different. Figure 4a shows the current-time response of $Li[Li_{0.2}Co_{0.3}Mn_{0.5}]O_2$ electrode in $LiAsF_6$/EC+DMC for a small potential step from 3.60 to 3.55 V. This potential corresponds to the CV peak potential of $Li[Li_{0.2}Co_{0.3}Mn_{0.5}]O_2$ electrode in the same electrolyte as shown in Figure 1b. It can be seen clearly that in the nonaqueous solution the current response for the applied potential step is much lower than that in the aqueous electrolyte solution due to the low ionic conductivity of organic-based solutions, which is in good agreement with the CV results obtained for $Li[Li_{0.2}Co_{0.3}Mn_{0.5}]O_2$ electrode in aqueous and nonaqueous electrolytes. Figure 4b shows the $It^{1/2}$ vs. log t plot calculated from the data of Figure 4a. This

curve has a minimum (approaching Cottrell behavior) at a longer time as compared to that observed with the aqueous electrolyte. This once again confirms the slow kinetics of lithium-ion intercalation from the nonaqueous electrolyte as compared to that from aqueous solutions. A similar trend is observed in the case of other plots (Figure 4c and 4d) calculated from the same data. The value of diffusion coefficient calculated from the inverse plot (Figure 4d) using Eq. 9 was found to be 2.05×10^{-11} cm^2 s^{-1}, which is one order of magnitude lower than that determined with aqueous electrolyte.

GITT studies

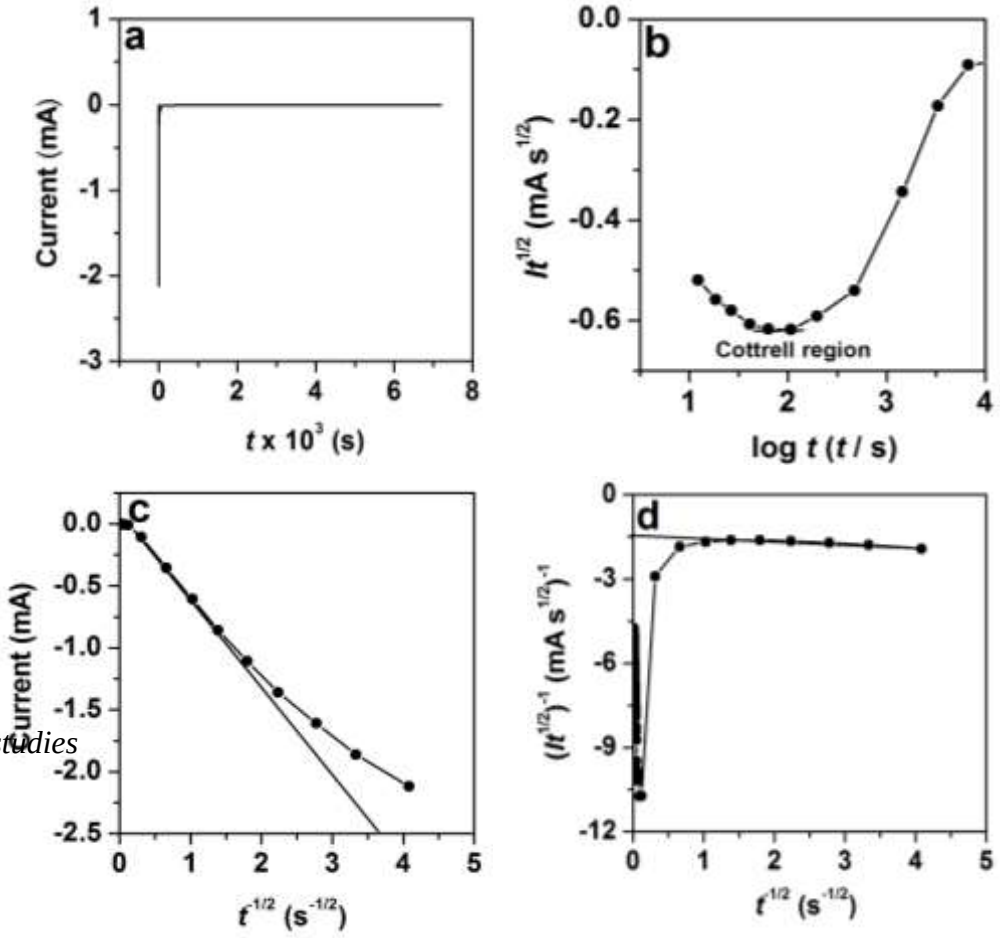

Figure 4. (a) Typical chronoamperometric curve of $Li[Li_{0.2}Co_{0.3}Mn_{0.5}]O_2$ electrode in1 M $LiAsF_6$ / EC+DMC organic electrolyte. The potential step used was 3.60 to 3.55 V (vs. Li/Li^+). (b) $It^{1/2}$ vs. log t (c) I vs. $t^{-1/2}$ (d) $(It^{1/2})^{-1}$ vs. $t^{-1/2}$ plots calculated from the data of Figure 4a.

As mentioned already, GITT predicts a linear relationship between the potential and the square root of time in the short time range of the galvanostatic potential transient, whereas PITT measurements deviate from the linear relationship between current and inverse square root of time due to numerous reasons. Therefore, it seems appropriate to determine the lithium ion diffusivity of $Li[Li_{0.2}Co_{0.3}Mn_{0.5}]O_2$ electrode as a function of lithium content by using the GITT technique. In this regard, we have measured a sequence of voltage responses from the $Li[Li_{0.2}Co_{0.3}Mn_{0.5}]O_2$ electrode upon the imposition of intermittent constant-current pulses of 0.1 mA, each for a period of 600 s. As an example, Figure 5a shows typical E vs. $t^{1/2}$ plot measured from $Li[Li_{0.2}Co_{0.3}Mn_{0.5}]O_2$ electrode after application of 0.1 mA current pulse. The linear relationship with a positive slope shown in the Figure verifies the short-time approximation ($t << l^2/D$) for semi-infinite diffusion process and confirms the validity of Eq. 6 for calculating the chemical diffusion coefficient of lithium ions in $Li[Li_{0.2}Co_{0.3}Mn_{0.5}]O_2$ electrode. The chemical diffusion coefficient of lithium ions in the electrode can be calculated from the slope of this curve. The corresponding differential curve is additionally plotted on the same Figure. The slope of this curve remains constant with the time range for the applied current pulse which indicates a pure diffusion process. However, the linearity of E vs. $t^{1/2}$ holds true as a first approximation only. The slope of the differential curve remains constant with the time range at lower applied current pulses only. When the applied current pulse is higher, the slope of $dE/dt^{1/2}$ plot does not remain constant. The polarization increases faster than Eq. 12 predicts; evidence of the existence of additional contributing kinetic factors besides pure diffusion [30]. A positive slope of $dE/dt^{1/2}$ plots were obtained for intercalation electrodes such as $LiFePO_4$, when studied with nonaqueous electrolytes [30]. This observation was explained by a theoretical approach which predicts the existence of SEI which causes a slow interfacial lithium-ion transfer across the SEI–particle boundary. The surface inhibition due to SEI generates a difference between the concentration levels on both

sides of SEI. The absence of this behavior (positive slope of $dE/dt^{1/2}$ plots) in our study once again confirms the absence of such slow interfacial ion transfer in aqueous electrolytes. Figure 5b shows the voltage response and corresponding differential plot versus square root of time obtained for $Li[Li_{0.2}Co_{0.3}Mn_{0.5}]O_2$ electrode in nonaqueous electrolyte around the CV peak potential. As expected, potential varies linearly with a positive slope similar to that observed with aqueous electrolyte. However, the variation of $dE/dt^{1/2}$ with a slope was observed in nonaqueous electrolyte, which can be attributed to the retardation of charge transfer across SEI. The parameters ΔE_{SEI} (polarization in the SEI) and R_{SEI} (the electric resistance of SEI) concern this interface. A mathematical formulation of lithium transport and a detailed analysis of the experimental observations through this interface were reported by Churikov et al. [30].

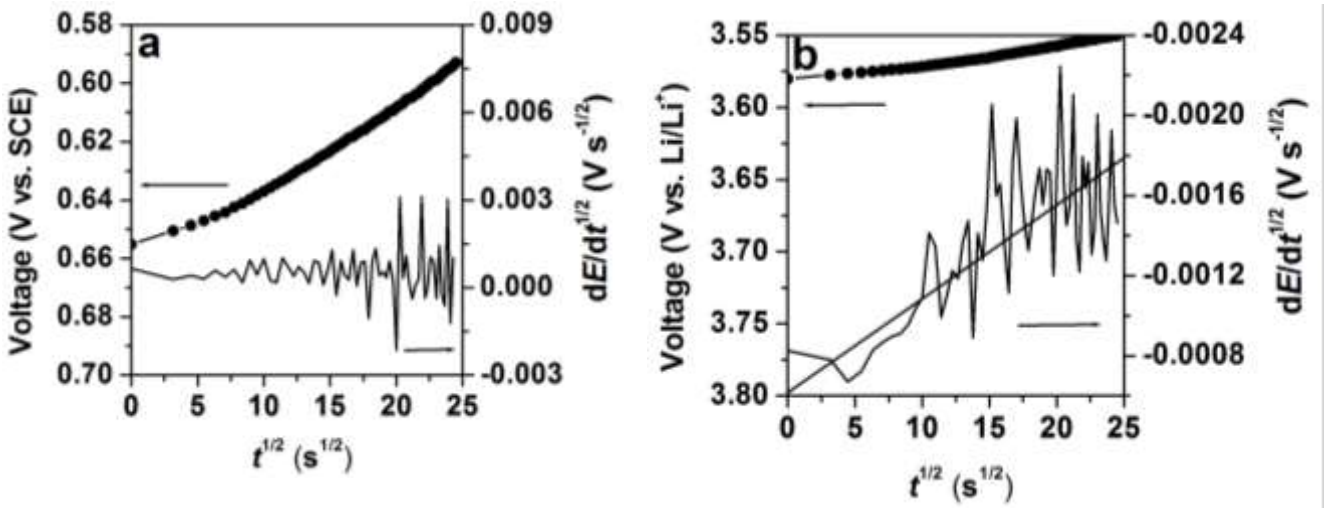

Figure 5. The plot of E versus $t^{1/2}$ and the corresponding differential curves measured from $Li[Li_{0.2}Co_{0.3}Mn_{0.5}]O_2$ electrode in (a) 2 M Li_2SO_4 aqueous electrolyte (b) 1 M $LiAsF_6$ / EC+DMC nonaqueous electrolyte by GITT.

Solid-state diffusion kinetics studied by simultaneous application of SSCV, PITT and GITT

Elucidation of the complexity of lithium intercalation into ion insertion electrodes is only possible based on simultaneous analysis of the dependence of voltage on the intercalation

capacity (C_{int}) obtained by appropriate electroanalytical techniques such as slow-scan rate cyclic voltammetry (SSCV), PITT and GITT. The process of ion insertion into host electrodes that have been polarized in solutions can be regarded as first-order phase transitions. Therefore, the chemical diffusion coefficient measured in parallel to C_{int} may shed new light on the nature of phase transitions under consideration. In this regard, we have plotted the intercalation capacity curves of the $Li[Li_{0.2}Co_{0.3}Mn_{0.5}]O_2$ electrode in the potential range 0.2 – 1.0 V, measured by SSCV at a scan rate of 0.1 mV s^{-1}; by PITT using 20 mV potential steps (in the vicinity of the minima on C_{int} vs. E curves, the potential steps during titration were as small as 10 mV); and by GITT using a current pulse of 0.1 mA. Figure 6 presents these three sets of incremental capacity curves of $Li[Li_{0.2}Co_{0.3}Mn_{0.5}]O_2$ electrode measured in 2 M Li_2SO_4 aqueous electrolyte. The electrode incremental capacity was calculated as $C_{int} = I/v$ (CV), $C_{int} = \Delta Q/\Delta E$ (PITT), where ΔQ is the change in the amount of charge inserted after application of a small potential step ΔE and $C_{int} = I\Delta t_p/\Delta E$ (GITT), where Δt_p is the galvanostatic pulse duration. These curves resemble each other extensively. All three curves have similar minima, although the resolution of responses with respect to potential turns out to be different. The half-peak width of all the peaks is approximately the same for all the three curves. These curves reflect different states of the intercalation electrode in connection with their approach to quasi-equilibrium. Further, the Figure reveals that the resolution of GITT is almost the same as that of PITT. Some discrepancy between these two curves can be attributed to the different conditions for the lithium intercalation in these methods. Peaks of C_{int} measured by PITT are shifted towards less positive potentials compared with the peaks measured by CV. The most important feature of the peaks in Figure 6 is their relatively narrow width. These narrow peaks may be understood if we consider the possibility of an attractive interaction between the inserted species at their sites. The intercalated lithium ions tighten the $Li[Li_{0.2}Co_{0.3}Mn_{0.5}]O_2$ layers together, resulting in the

formation of clusters which can be considered as charge transfer between lithium and the transition metal oxide layers. Hence the intercalation process can be explained by considering the possible attractive interaction of the inserted species in terms of the Frumkin-type intercalation isotherm as well as non-equilibrium charging of both the Li–composite and composite–solution interfaces. i.e., the isotherm which is widely used to describe adsorption process in which there is strong interactions in the adsorption sites can also describe the intercalation process which occurs in the bulk. Hence, the adsorption isotherm can be used to describe intercalation phenomena and they may be called isotherm of intercalation. A general equation for the intercalation isotherm has the following form [33]:

$$a_{h,Li+} = \beta a_{s,Li+} \tag{10}$$

where, $a_{h,Li+}$ and $a_{s,Li+}$ are the activity of lithium ion in the host and solution, respectively, and β is a constant which is a function of the electrode potential. It is assumed that the intercalation level of lithium ions into the inorganic host materials results in a certain change in their interaction energy. In this case Eq. 10 changes to [33]:

$$a_{h,Li+} = [x/(1-x)]\exp(-gx) = \beta a_{s,Li+} \tag{11}$$

with g representing a dimensionless constant, which is a measure of mean interaction energy between the intercalation sites (positive for repulsion and negative for attraction), and x is the intercalation level in the host bulk. However, there is an important difference between the features of intercalation and adsorption process. For the intercalation process, equilibrium consideration includes the distribution of both electronic and ionic species within the host bulk, whereas the adsorption process is related to the ionic species only. The presence of two kinds of species during intercalation results in a more complicated picture of potential distribution in the host bulk and across the metal–host and host–solution interfaces, as compared with such distribution in the case of adsorption [33].

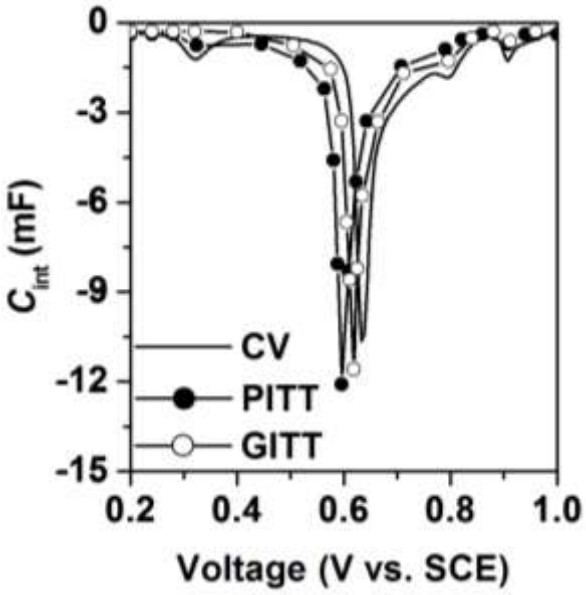

Figure 6. Variation of incremental capacity with potential for $Li[Li_{0.2}Co_{0.3}Mn_{0.5}]O_2$ electrode from 2 M Li_2SO_4 aqueous electrolyte measured by CV, PITT and GITT.

Figure 7 compares the log *D* vs. *E* plot of $Li[Li_{0.2}Co_{0.3}Mn_{0.5}]O_2$ electrode obtained by PITT and GITT in the range of potentials 0.2 to 1.0 V. The chemical diffusion coefficient was calculated using Eq. 9 and Eq. 7 from PITT and GITT, respectively. The two curves shown in this figure are in reasonable agreement. One can see that the potentials of minima on the log *D* vs. *E* correspond well with the peak potentials of the C_{int} vs. *E* curve shown in Figure 6. The minima on the log *D* vs. *E* and C_{int} vs. *E* curves are assumed to reflect attractive interactions between the intercalation species. These peaks relate to phase transition and thus corresponding minima on the log *D* vs. *E* curve should be the most pronounced. This is correct if the potential step used is much less than the half-peak widths on the C_{int} versus *E* curve (potential step use was 10 mV, whereas half-peak width is about 25 mV). However, the relatively narrow C_{int} peaks and minima in log *D* vs. *E* at the peak potentials in this potential range are typical of lithium insertion processes with attractive interaction in the intercalation sites. According to Mc Kinnon [21], long range repulsive interaction site leads to broad peaks

in the electrode votammogramms. During short range repulsive interactions, we may obtain an intercalation reaction which proceeds via disorder-order-disorder transitions. In such cases, the votammogramms of this process is characterized by two narrow peaks with a minimum in between, which corresponds to the ordered structure. Thus, short-range repulsive interactions may lead to lithium intercalation which proceeds via consecutive two-phase transitions with an apparent electro analytical response similar to that described in terms of short-range attractive interactions. Application of a small incremental charge into a two-phase system with a distinctive boundary between the phases shifts this boundary towards the interior of the active mass particles. The chemical diffusion coefficient in this case should effectively reflect the highly attractive interaction between the intercalation sites in this narrow region. It should be remembered that the calculations of the kinetic parameters such as diffusion coefficient of ion insertion electrodes are based on solutions of Fick's laws, which are mostly suitable for single phase transitions. However, intercalation of lithium ion into the cathode materials like $Li[Li_{0.2}Co_{0.3}Mn_{0.5}]O_2$ are accompanied by phase transitions at different potential domains in which two phases coexist. In these cases, Fick's laws are not exactly fulfilled. However, in most cases the potential domains in which the two phases coexist are very narrow, and can be considered negligible, compared with the entire voltage domain of interest in which the diffusion coefficient is measured. The minimum observed in the plots of log *D* vs. *E* curve relates to this narrow region. In this narrow domain many systems show pseudo-Cottrell behavior, and hence the diffusion coefficient determined in this narrow potential domain can be considered as an apparent diffusion coefficient, relevant only to this domain. In all other potential domains true values of *D* can be calculated [33].

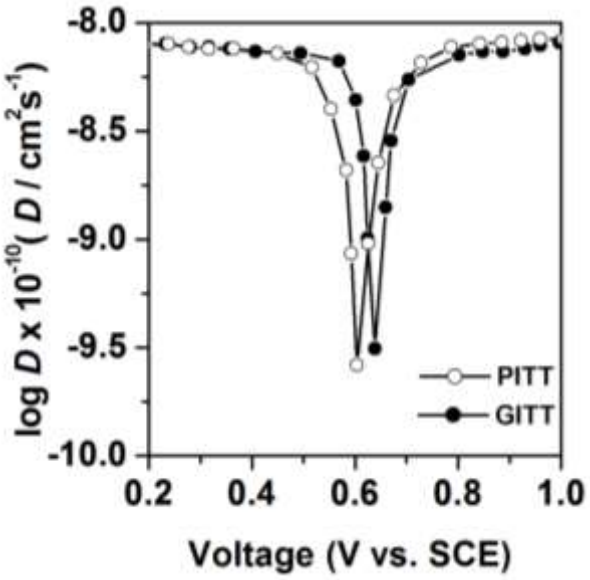

Figure 7. Dependence of the chemical diffusion coefficient of lithium ions on potential obtained by PITT and GITT from $Li[Li_{0.2}Co_{0.3}Mn_{0.5}]O_2$ electrode in 2 M Li_2SO_4 aqueous electrolyte.

Conclusions

PITT and GITT have been applied to $Li[Li_{0.2}Co_{0.3}Mn_{0.5}]O_2$ electrode in order to obtain highly resolved plots of incremental capacitance and chemical diffusion coefficient versus potential from an aqueous electrolyte. The intercalation-deintercalation reaction related to this electrode belongs to a topotactic solid-state reaction appearing in the form of solid solution formation. Using a simple analysis of the dependence of the PITT parameter ($It^{1/2}$) and slope of E vs. $t^{1/2}$ curve from GITT on the intercalation isotherm, it was shown that both techniques should lead to the same D vs. E relationship. The correspondence between the peaks of the intercalation capacitance and the minima in the log D vs. E curve is explained via an approach which describes lithium intercalation into host materials in terms of Frumkin isotherm. The behavior in C_{int} and log D vs. E plots is related to short-range attractive interactions amongst the intercalation sites. These results are in good agreement with the literature data reported for these types of layered cathode materials. The information obtained

from these studies can greatly enhance our understanding of the battery performance and deficiencies of this cathode material for future improvements.

Acknowledgement

The authors gratefully acknowledge the financial support from the Science and Engineering Research Board, New Delhi. Authors wish to thank Sri. A. V. S. Murthy, honorary secretary, Rashtreeya Sikshana Samiti Trust, Bangalore, for his support and encouragement. We are grateful to Prof. N. Munichandraiah, Inorganic and Physical Chemistry department, IISc, Bangalore for helping us to carryout nonaqueous experiments. K. C. Mahesh thanks the management and staff of Mount Carmel College, Autonomous, Vasanth Nagar, Bangalore for their encouragement.

References

1. Armstrong AR , Bruce PG (1996) Nature 381:499–500
2. Armstrong AR, Huang B, Jennings RA, Bruce PG (1998) J Mater Chem 8:255–259
3. Shao-Horn Y, Hackney SA, Armstrong AR, Bruce PG, Gitzendanner R, Johnson CS, Thackeray MM, (1999) J Electrochem Soc 146:2404–2412
4. Lu Z, MacNeil DD, Dahn JR (2001) Elctrochem Solid State Lett 4:A191–A194
5. Lu Z, Dahn JR (2002) J Electrochem Soc 149:A815–A822
6. Lu Z, Dahn JR (2002) J Electrochem Soc 149:A1454–A1459
7. Kim JS, Johnson CS, Thackeray MM (2002) Electrochem Commun 4:205–209
8. Ohzuku T, Nagayama M, Tsuji K, Ariyoshi K (2011) J Mater Chem 21:10179–10188
9. Bareno J, Lei CH, Wen JG, Kang SH, Petrov I, Abraham DP (2010) Adv Mat 22:1122–1127
10. Ellis BL, Lee KT, Nazar LF (2010) Chem Mat 22:691–714
11. Park YJ, Hong YS, Wu X, Kim MG, Ryu KS, Chang SH (2004) J Electrochem Soc 151:A720–A727

12. Lu Z, Beaulieu LY, Donaberger RA, Thomas CL, Dahn JR (2002) J Electrochem Soc 149:A778–A791

13. Kang SH, Sun YK, Amine K (2003) Elctrochem Solid State Lett 6:A183–A186

14. He W, Qian J, Cao Y, Ai X, Yang H (2012) RSC Adv 2:3423– 3429

15. Armstrong AR, Holzapfel M, Novak P, Johnson CS, Kang SH, Thackeray MM, Bruce PG (2006) J Am Chem Soc 128:8694–8698

16. Xu B, Fell CR, Chi MF, Meng YS (2011) Energy Environ Sci 4:2223–2233

17. Ito A, Li D, Sato CY, Arao M. Watanabe M, Hatano M, Horie H, Ohsawa Y (2010) J Power Sources 195:567–573

18. Gao J Manthiram A (2009) J Power Sources 191:644–647

19. Arunkumar TA, Alvarez E, Manthiram A (2008) J Mat Chem 18:190–198

20. Han BC, Van der Ven A, Morgan D, Ceder G (2004) Electrochim Acta 49:4691–4699

21. McKinnon WR, Haering RR (1983) Modern aspects in electrochemistry. Plenum, New York.

22. Levi MD, Aurbach D (2007) J Solid State Electrochem 11:1031–1042

23. Wen CJ, Boukamp BA, Huggins RA (1979) J Electrochem Soc 126:2258–2266

24. Deiss E (2002) Electrochim Acta 47:4027–4034

25. Varsano F, Decker F, Masetti E, Croce F (2001) Electrochim Acta 46:2069–2075

26. Weppner W, Huggins RA (1977) J Electrochem Soc 124:1569–1578

27. Choi YM, Pyun SI (1998) Solid State Ionics 109:159–163

28. Levi MD, Levi EA, Aurbach D (1997) J Electroanal Chem 421:89–97

29. Eftekhari A (2001) Electrochim Acta 47:495–499

30. Churikov AV, Ivanishchev AV, Ivanishcheva IA, Sycheva VO, Khasanava NR, Antipov EV (2010) Electrochim Acta 55:2939–2950

31. Montella C (2002) J Electroanal Chem 518:61–83

32. Vorotyntsev MA (2004) J Electroanal Chem 572:299–307

33. Levi MD, Aurbach D (1999) Electrochim Acta 45:167–185